JAST
Journal of Aerospace Science and Technology

Pages: 137- 150 / Vol. 16/ Issue 2 / Summer- Fall 2023

Journal of Aerospace Science and Technology

www:jast.ias.ir

Scientific-Research Article

An enhanced Lattice-Boltzmann method for speeding numerical solutions

Motreza Bayati[1]

1- Department of Aerospace Engineering, Urmia University of Technology ,Urmia, Iran

ABSTRACT

Keywords: *Lattice-Boltzmann, channel, convergence speed, flow*

Minimizing the computational cost and improving the convergence speed is the main goal of any computational design. In this regard, a new method to improve the traditional iterative method of fluid flow solution is applied due to the low convergence speed of the traditional iterative method. In this paper, two-dimensional fluid flow in a channel with an aspect ratio of 10, uniform inlet velocity, constant outlet pressure, and no-slip conditions at the walls is studied using the Lattice-Boltzmann Method. The solution's convergence speed is increased by verifying that the mass flux is conserved between the inlet and each channel section. The solution time of channel flow obtained by the Lattice-Boltzmann Method for Reynolds number of 100 and three types of grids 40x400, 60x600, and 80x80 are 261, 1039, and 4264 s, respectively. Based on the results, introducing a flow rate control in each channel section of these three grids reduces the solution time by 35, 266, and 1590 seconds. This method can be implemented not only for normal channels but also for channels with obstacles. According to the results, the speed of convergence increases by at least 2 times using this method.

Nomenclature

c	Lattice streaming speed
c_s	sound speed
D	width of channel
L	length of channel
e_k	discrete particle velocity
f_k	distribution function
f_k^{eq}	equilibrium distribution function
H	height of channel
k	direction index in LBM (0…9)
dA	area of element
$\dot{m}_{in}$	inlet mass flow rate
$\dot{m}_{section}$	mass flow rate at every cross section
P	fluid pressure
n	factor of time
Re	Reynolds number ($U_{in} \cdot D/v$)
URF	Under Relaxation Factor
$\boldsymbol{u}$	fluid velocity vector
U	dimensionless velocity (u/u_{in})
u_{in}	inlet fluid velocity
u	x-velocity of fluid
v	y-velocity of fluid
x	horizontal axial
y	vertical axis
X	non dimensional x-coordinate (x/D)
Y	non dimensional y-coordinate (y/D)
$\boldsymbol{x}$	particle position vector

1 Assistant Professor

10.22034/jast.2023.376159.1139

Submit: 10.12,2022/ Accepted: 29.07.2023

Print ISSN:2345-3648 Online ISSN: 1735-2134

Greek symbols

ν	kinematical viscosity
Δx	space step
Δt	time interval
τ_F	relaxation time
w_k	weighting coefficient
ρ_0	density of fluid at the outlet
ρ	density of fluid

Introduction

In general, numerical methods are used to solve complex fluid mechanics problems. The domain is divided into small elements and grids in all these methods. These models require more elements to achieve high response accuracy. On the other hand, increasing the number of elements increases the solution time. The Lattice Boltzmann Method (LBM) has emerged as a powerful computational tool for simulating fluid flow.

Measurement of fluid flow in channels is one of the most common problems in fluid dynamics involved in various industrial processes. This problem usually has obstacles, etc. In this case, a higher factor is required. As mentioned earlier, increasing the number of elements increases the time required to complete the simulation. Although many methods have been developed to reduce the resolution time, parallelizing is one of them. In numerical methods for solving fluid flow problems, all the published solution algorithms, including the prediction method [1], the simple algorithm [2-5], the coupled method [6-9], the synthetic compression method [10], the velocity flow function [11], the submerged boundary method [11], have determined the pressure level for pressure control [12]. While the momentum equations retain their role in determining the velocity field. In addition, the LBM [13, 14], a mesoscopic method based on kinetic theory, has been used to simulate incompressible fluid flow in recent years. Over the years, significant progress has been made in refining and enhancing the LBM to improve its accuracy, efficiency, and applicability to a wide range of complex flow phenomena. A new discretized pressure Poisson algorithm for the steady incompressible flow based on a non-staggered grid has been studied by Lou and Ren [15]. Choudhury has studied the unsteady hydrodynamic free convective flow of a viscoelastic incompressible fluid past a vertical porous plate in the presence of a variable suction [16]. Ashrafi investigated the performance of PEMFCs with different geometries under different operating conditions [17]. Incompressible fluid flow characteristics in the field of ship and ocean engineering have been investigated by Fan [18]. The power-law fluid flow in the trapezoidal cavity has been conducted using Chen's incompressible finite-difference lattice Boltzmann method [19]. Three-dimensional simulations of incompressible flows in oscillating cubic lid-driven cavities have been simulated by LBM that focuses on examining the impact of Reynolds number and oscillating frequency on the flow field [20]. Progress in LBM for incompressible fluid flow can be mentioned in the following. Combining the LBM with a convolutional neural network and a gated recurrent unit neural network improves speed and convergence [21]. In Yang's [22] work, a study was done on LBM with two relaxation time models, and its efficiency was compared with LBM with a single relaxation time model for predicting effective thermal conductivity. A mesh refinement methodology was proposed for simulating phase-change heat transfer problems employing the pseudopotential LBM, which was based on relating the physical parameters to their lattice counterparts for an arbitrary mesh under the viscous regime in LBM [23].

This paper uses a novel method that utilizes steady, two-dimensional, incompressible, and laminar flow mechanics relations to reduce the solution time for determining the flow field. Previous studies have shown that the iteration of the velocity equation and the pressure control equation can accelerate the convergence of the pressure control algorithm [24]. Bloch [25] investigated the mass correction in the compression correction algorithm. Bloss's paper shows that the pressure gradient in the two channels can be solved by the finite element method, and the coupling speed can be improved by adjusting the mass flow. In the Blush model, mass correction is performed only on the output boundary, and no correction is performed throughout the domain. This work checks the mass correction on the entire solution space. By correcting the flow rate inside the channels, the convergence speed of the problem increases by more than two times.

Geometry

Figure (1) shows the geometry of the problem used in this paper. In Figure (1), D is the inlet channel width, and L is the channel length, which is ten times the inlet channel width. Also, in Figure (1), (X=x/D) is the distance from the inlet, and (Y=y/D) is the

distance from the bottom wall, which is dimensionless by the channel width.

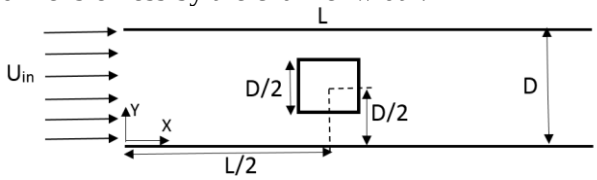

Fig. 1: Problem geometry consists of a dimensionless channel and an obstacle

According to Figure (1), the geometry of this problem includes a 2-dimensional channel with a square obstacle, which is located at a distance (X=5, Y=0.5) from the origin coordinates. All of the parameters of the channel become dimensionless with inlet channel width.

The method of solution

Lattice-Boltzmann method

This paper uses a 2-dimensional, 9-directional (D2Q9) Lattice-Boltzmann method to solve the fluid flow. It is worth mentioning that the LBM has some pronounced advantages convincing the researchers to use this method. The advantages of LBM can be mentioned, such as linear stability in parallel computing, which makes this method more accurate due to local collision calculation. Moreover, this method can handle complex geometry and accurately simulate the fluid flow and heat transfer of incompressible flows. The major advantage of LBM over other conventional CFD methods is that the solution for the particle distribution functions is explicit, and the implementation of boundary conditions on complex boundaries is simple. The LBM originated from the lattice gas automata, which are discrete models for the simulation of transport phenomena. In these models, the computational grid consists of several lattice points that are connected with some of their neighboring sites by a bond or link. At each time step, particles move synchronously along the bonds of the lattice and interact locally, subject to physical conservation laws [26]. This model and the method for the selection of the directions are shown in Figure (2).

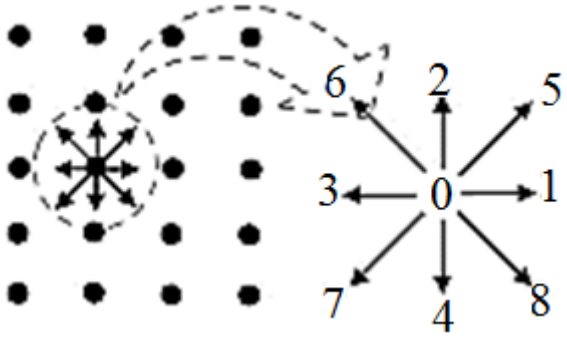

Fig. 2: Lattice-Boltzmann Directions

In the D2Q9 model, particles will be able to move in 8 directions, which are determined by Figure (2), or remain stationary at zero point and have no displacement.

Governing equations

The momentum equation is rewritten as follows using the Lattice-Boltzmann equation and the estimation of the collision term of the Bhatnagar–Gross–Krook (BGK) equation.

$$f_k(\boldsymbol{x} + e_k \cdot \Delta t.\mathrm{t} + \Delta \mathrm{t}) - f_k(\boldsymbol{x}.\mathrm{t}) = -\frac{1}{\tau_F}\left(f_k(\boldsymbol{x}.\mathrm{t}) - f_k^{eq}(\boldsymbol{x}.\mathrm{t})\right) \quad (1)$$

In Eq. (1), f is the distribution function for the velocity. The distribution functions of f can be obtained by solving the lattice Boltzmann equations for velocity fields. $\Delta \mathrm{t}$ is the time interval, f^{eq} is the function of equilibrium distribution, e_k is the unit vector of transposition, τ_F is the relaxation time. The value of k is the parameter that determines the direction of the lattice (k=0, 1, 2, 3, 4, 5, 6, 7, 8). The unit vector, e_k is defined as follows.

$$e_k = \begin{cases} 0 & k = 0 \\ \left(cos\left(\frac{\pi}{2}(k-1)\right).sin\left(\frac{\pi}{2}(k-1)\right)\right) & k = 1,2,3,4 \\ \sqrt{2} \times \left(cos\left(\frac{\pi}{2}\left(k-\frac{9}{2}\right)\right).sin\left(\frac{\pi}{2}\left(k-\frac{9}{2}\right)\right)\right) & k = 5,6,7,8 \end{cases} \quad (2)$$

The parameter f^{eq} is determined as follows:

$$f_k^{eq}(\boldsymbol{x},t) = w_k \cdot \rho \cdot \left[1 + 3\frac{e_k \cdot \boldsymbol{u}}{c^2} + \frac{9}{2}\frac{(e_k \cdot \boldsymbol{u})^2}{c^4} - \frac{3}{2}\frac{\boldsymbol{u}^2}{c^2}\right] \quad (3)$$

In Eq. (3), the value of w_k is a weighting function that varies in different directions, and ($c = \frac{\Delta x}{\Delta t}$) is the Boltzmann constant. ρ is the density, and $\boldsymbol{u}$ is the velocity of the fluid, and both of them are in terms of the Lattice units. Weight function, w_k is defined as follows.

$$w_k = \begin{cases} \frac{4}{9}. & k = 0 \\ \frac{1}{9}. & k = 1,2,3,4 \\ \frac{1}{9}. & k = 5,6,7,8 \end{cases} \quad (4)$$

And also, microscopic velocity and density are obtained from the following relations:

$$\rho = \sum_{k=0}^{8} f_k \quad (5)$$

$$\boldsymbol{u} = \frac{1}{\rho}\sum_{k=0}^{8} f_k \cdot e_k \quad (6)$$

In the *D2Q9* model, the pressure of fluid is determined from the density as follows.

$$P = c_s^2 \cdot \rho \quad (7)$$

where c_s is the speed of sound, which is obtained from the following relation.

$$c_s = \frac{c}{\sqrt{3}} \quad (8)$$

The fluid kinematic viscosity is determined as follows [27];

$$v = \frac{c^2}{3}\left(\tau_F - \frac{1}{2}\right) \quad (9)$$

where τ_F is the relaxation time, and c is the Lattice constant, which is equal to one in this paper. For the state where there is no obstacle, the Reynolds number is defined as:

$$\mathrm{Re} = \frac{U_{in}D}{\nu} \quad (10)$$

where U_{in} is the inlet channel velocity, D is the size of the width, and ν is fluid kinematic viscosity. If an obstacle is added to the geometry of the model, D is the width size of the square.

Boundary condition

In this part, according to Figure (3), the function of distributions with an inward component are considered boundary conditions and must be included.

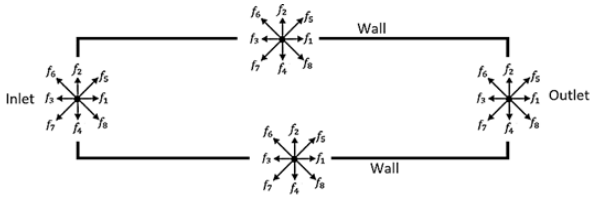

Fig. 3: The definition of walls, inlet, outlet, and computational domain

Inlet boundary condition

The inlet boundary condition is defined using a uniform flow as follows [28].

$$\rho = \frac{(f_0 + f_1 + f_3) + 2 \times (f_3 + f_7 + f_6)}{1 - u_{in}} \quad (11)$$

$$f_1 = f_3 + \frac{2}{3}\rho \cdot u_{in} \quad (12)$$

$$f_5 = f_7 + \frac{1}{6}\rho \cdot u_{in} - \frac{1}{2}(f_2 - f_4) \quad (13)$$

$$f_8 = f_6 + \frac{1}{6}\rho \cdot u_{in} - \frac{1}{2}(f_4 - f_2) \quad (14)$$

Outlet boundary condition

Outlet boundary condition is defined using pressure as follows [29].

$$u = -1 + \frac{(f_0 + f_2 + f_4) + 2 \times (f_1 + f_5 + f_8)}{\rho_0} \quad (15)$$

$$f_3 = f_1 - \frac{2}{3}\rho_0 \cdot u \quad (16)$$

$$f_6 = f_8 - \frac{1}{6}\rho_0 . u + \frac{1}{2}(f_4 - f_2) \quad (17)$$

$$f_7 = f_5 - \frac{1}{6}\rho_0 \cdot u + \frac{1}{2}(f_2 - f_4) \quad (18)$$

Walls boundary condition

Wall boundary conditions and obstacle walls are defined using the bounce-back model. Bounce-back model is a no-slip condition [29].
For the upper wall of the channel:

$$f_4 = f_2 \quad (19)$$

$$f_8 = f_6 \quad (20)$$

$$f_7 = f_5 \quad (21)$$

For the bottom wall of the channel:

$$f_2 = f_4 \quad (22)$$

$$f_6 = f_8 \quad (23)$$

$$f_5 = f_7 \quad (24)$$

Fluent software

Fluent software is used to compare the required time for the solution of the channel problem [30]. The boundary conditions and the geometry were simulated in Fluent software are shown in Figure (4).

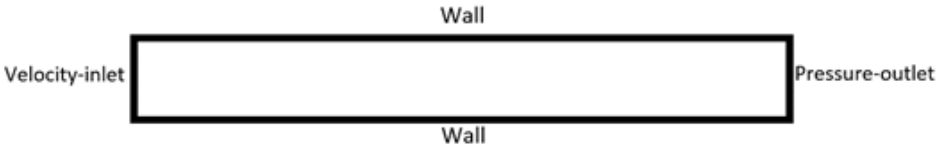

Fig. 4: Boundary conditions of Fluent model

Flow rate control code

In steady state numerical simulation, the computational domain is initiated to specify the flow field velocity distribution. However, the initial values could be very different from the final correct values. On the other hand, the velocity at the inlet boundary condition remains constant over the time of the solution calculations. Therefore, the amount of mass flow rate calculated at the input boundary will remain constant. Since the velocity of the elements inside the computational domain is changed at the time of solving, the amount of mass flow rate at each section perpendicular to the channel axis will be different from the amount of flow rate at the entrance of the channel. So, in every time iteration, by this difference in mass flow rate in every cross section of the channel, the amount of velocity difference is calculated (according to equation 29) and can be summed to the total amount of the velocities which are located at that section (according to equation 28). This speeds up the solution and converges faster, significantly. Figure (4) also shows one section AA' perpendicular to the channel axis. The different cross sections are located in the direction of the channel axis with a distance of dx from each other. It should be noted that if the velocity difference due to the mass flow difference is added directly to the velocity of each section, it will cause instability of the solution and diverge. Therefore, the velocity difference should not be added directly to the velocity of the elements. To solve this problem, the velocity difference is added using the Under Relaxation Factor (URF) to avoid divergence.

Mathematical model

$$\dot{m}_{in} = \int_0^D \rho u_{in} dA \quad (25)$$

$$\dot{m}_{section} = \int_0^D \rho u_{section} dA \quad (26)$$

$$\frac{u_{section}^{new}}{u_{in}} = \frac{u_{section}^{old}}{u_{in}} + URF \times \frac{\frac{(\dot{m}_{in} - \dot{m}_{section})}{\rho}}{u_{in} \times D \times Re^2} \quad (27)$$

$$\frac{u_{section}^{new}}{u_{in}} = \frac{u_{section}^{old}}{u_{in}} + URF \times \Delta u^+ \quad (28)$$

$$\Delta u^+ = \frac{(\dot{m}_{in} - \dot{m}_{section})}{\rho \times u_{in} \times D \times Re^2} \quad (29)$$

where $\dot{m}_{in}$ is the inlet mass flow rate of the channel, ρ is the density of the fluid, u_{in} is inlet velocity, dA is the area of the surface element, $\dot{m}_{section}$ is cross-section mass flow rate, $u_{section}$is cross-section velocity distribution, and URF is the Under Relaxation Factor.

If the mass flow at the input section is greater than the mass flow at a cross-section within the calculation field, the velocity difference at that point will be positive, and this issue results in increasing the velocity on that cross-section and also results in increasing the convergence speed significantly. The convergence condition was that the residual reached below 10^{-4}. In all the test cases studied in this work, the initial velocity in the whole flow field, except the input boundary, is considered zero.

Results

Mesh independence

In order to determine the appropriate mesh number for a channel problem with an obstacle, three types of mesh, 40×400, 80×800, and 160×1600 have been solved by LBM with mass flow correction method, and then the dimensionless velocity distribution on the longitudinal axis of the channel (on the line X=2.5, 0<Y<1) has been shown and compared with each other.

Figure (5) shows the dimensionless velocity distribution in X= 2.5 coordinates for different types of meshes and a Reynolds number of 50. According to Figure (5), results for mesh 80×800, and 160×1600 are close to each other, so the mesh 80×800 is suitable for the model.

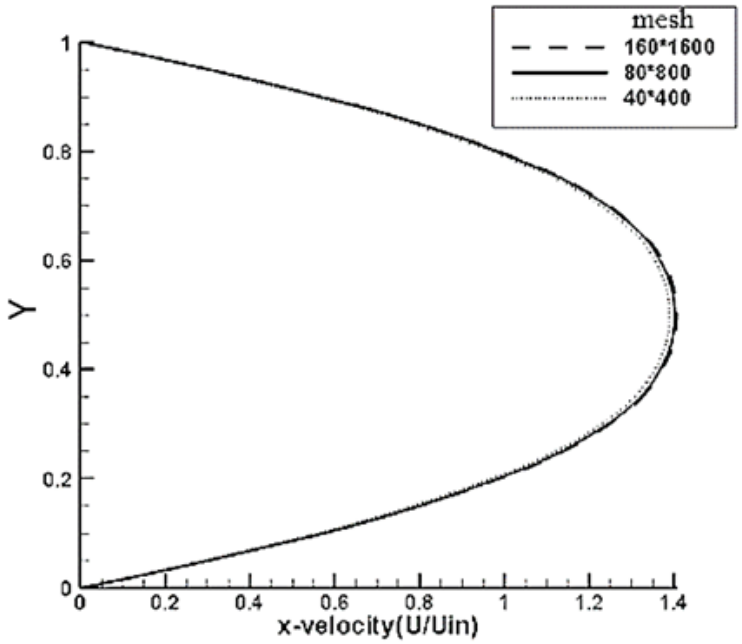

Fig. 5: Comparing the dimensionless velocity distribution for three different types of mesh

Validation

Figure (6) shows the geometry used in Breuer's paper [31]. According to Figure (6), a channel with a height of H, a length of L, and an obstacle with a width of D at the distance L from the inlet and H/2 from the bottom wall have been considered. The origin coordinate of this geometry was located at the center of the obstacle, and *l*/L=4, L/D=50. In their work, the problem was solved by using the numerical method of Lattice-Boltzmann and the finite volume method, and the results of these methods were compared with each other.

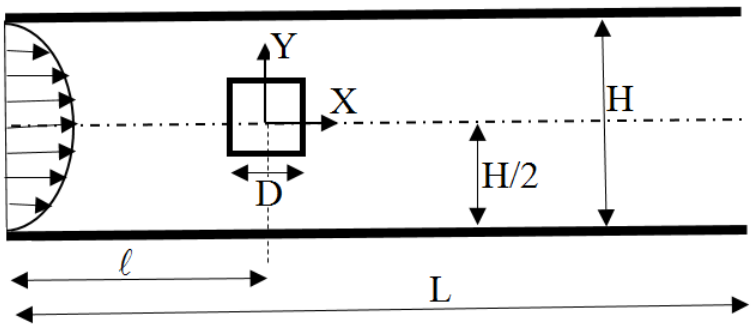

Fig. 6: The geometry of the paper released by Breuer [31]

In Figure (7), the results of axial velocity distribution (x-velocity) and vertical velocity distribution (y-velocity) on the horizon line (x, y=0) for Reynolds number of 100 have been shown and compared with the results of Breuer's paper [31]. According to Figure (7), at the entrance of the channel to the location of the obstacle, the value of vertical velocity (y-velocity) is zero. This is because of the symmetry of the geometry before the obstacle. After the obstacle, the vertical velocity (y-velocity) isn't zero, and it changes frequently due to the flow fluctuations and separation of vortices from the back of the obstacle.

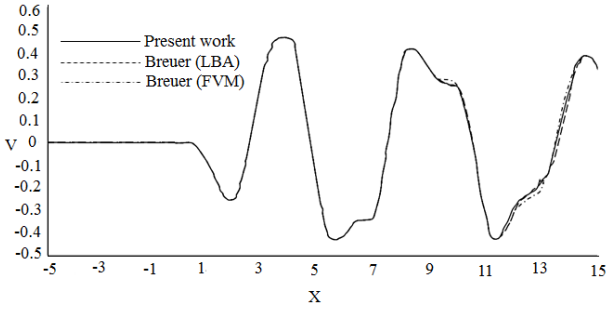

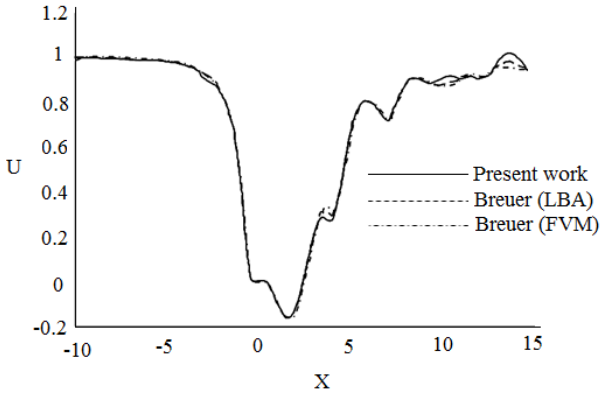

Fig. 7: Comparing the axial and perpendicular velocity distribution of present work with Breuer [31] on the core line with the coordinate of (x, y=0), in the channel with a dimension of H×L along with an obstacle with a dimension of D=L/50 and coordinate of (x=0, y=0).

Investigation of flow rate control on the number of mesh

In this part, a 2-D channel with length per width equal to 10 and *Re* = 100 for three types of mesh, 40×400, 60×600, and 80×800, have been solved for two states, flow rate control code, and without it, in all of the cases, the value of URF is 0.4. The results of the time required for these two types are shown in Figure (8). Computer CPU time was used to calculate the numerical computation time. According to Figure (8), the solution time is approximately related to the second power of the mesh increase ratio as the mesh number increases in all cases. The LBM solution time with flow control is less than 1/3 time in conventional LBM. This advantage is especially important in cases where the number of meshes is large.

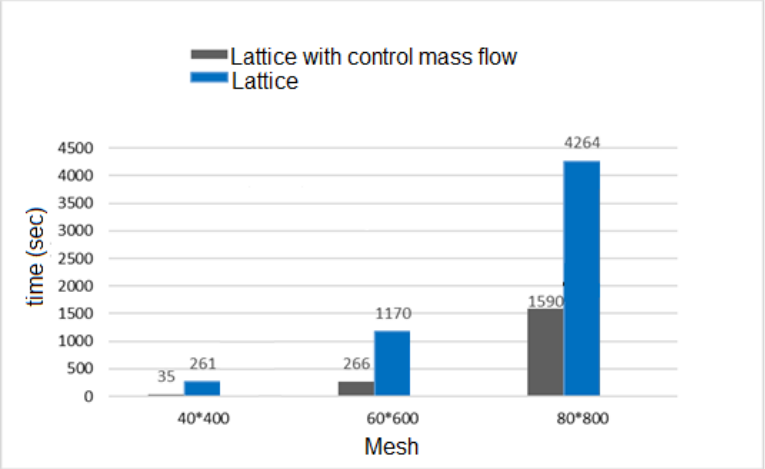

Fig. 8: Time required for the solution of the channel without the obstacle with three types of mesh, 40×400, 60×600, and 80×800, and URF=0.4

According to Figure (8), using a flow rate control code could increase the speed of convergence more than two times. This means that in problems that need high solution accuracy, this code is more significant. On the other hand, this method, in comparison to whole mass conservation, which is just considered the outlet of the channel, is more effective, and the speed of convergence would be higher by using flow rate control code.

Investigation of Under Relaxation Factor

In this part, a channel with a Reynolds number of 100 and mesh type of 40×400 for different values Under Relaxation Factor has been investigated. Figure (9) shows the URF in terms of iteration number until convergence.

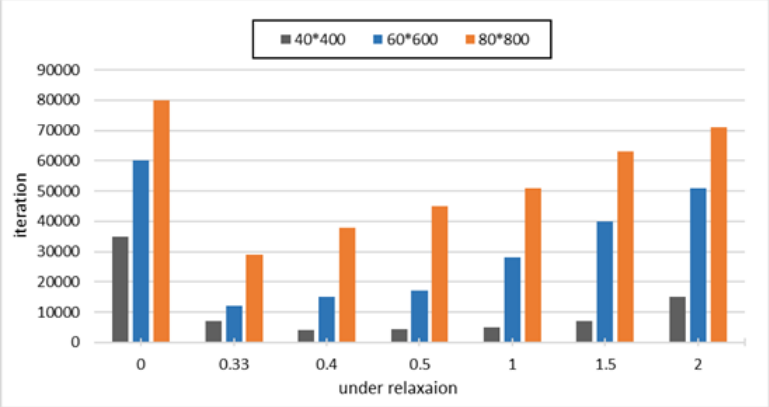

Fig. 9: Changes in URF in terms of iteration number until convergence for Reynolds number of 100 and mesh types of 40×400, 60×600, and 80×800 for channel without an obstacle.

According to Figure (9), an optimum value for URF is 0.4, It has the best convergence rate. Also, if the URF value exceeds 2, the solution diverges. Because in this case, by adding the amendment velocity to the old velocity of the element, the amount of velocity increase is too high and causes divergence.

Investigation of convergence speed in different Reynolds number

The convergence speed of problem solution in different Reynolds numbers in two states consisting of flow rate control and without control for mesh of 40×400 and URF of 0.4, has been shown in Figure (10).

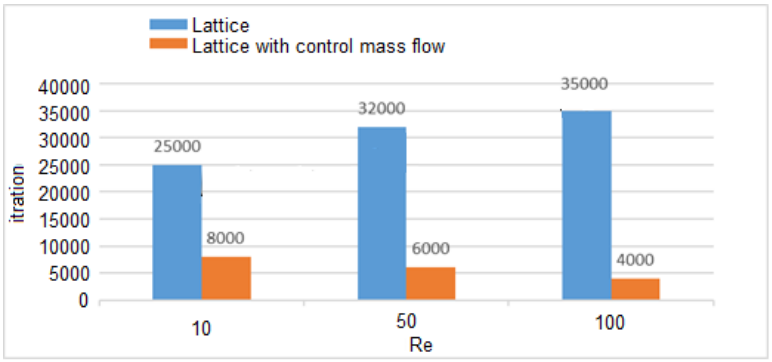

Fig. 10: The comparison of iteration number of problem solution for a channel without obstacle for mesh type 40×400 and with different Reynolds numbers, 10, 50, and 100 for two cases of flow rate control and without it.

In all of the Reynolds numbers the flow rate control code causes an increase in solution speed more than 2 times. Besides, by increasing the Reynolds number, the amount of iteration has been increased. In fact, by increasing the Reynolds number the stability of the problem has been reduced, and convergence needs more iteration. So, at a higher Reynolds number, the flow rate control code would be more effective.

The effect of flow rate control on channel with obstacle

In this part, a channel with a mesh of 80×800, length-to-width ratio = 10, and Reynolds number = 50, along with a square obstacle in the middle of the channel, have been considered. The geometry of the channel with square obstacle and boundary conditions has been shown in Figure (11).

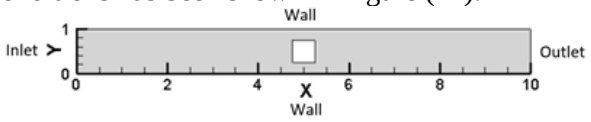

Fig. 11: Geometry of channel with square obstacle and boundary conditions, X and Y are non-dimensional axes

The ratio of channel width to the obstacle dimension is equal to 2. The results of the number of iterations for the channel with the obstacle for the two states, flow rate control and without it, have been shown in Figure (12).

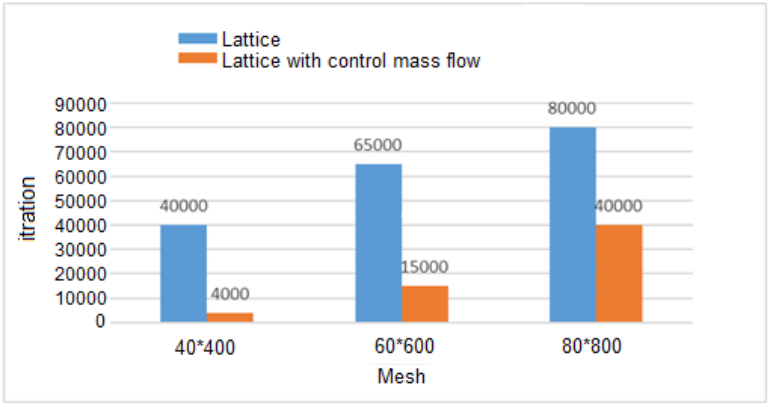

Fig. 12: Comparison of iteration number of solution problem for the channel with square obstacle for the two states of flow rate control, and without control.

According to Figure (12), by using flow rate control code in a channel with obstacle, the convergence speed is increased more than 2 times. Velocity distribution in different cross sections of channel with an obstacle for Reynolds number of 50 in two states, flow rate control and without it, shown in Figure (13). The difference between the two methods is below 0.5%. According to Figure (13), the results of these two solution methods are close to each other and in fact, converge to each other. The streamlines of the channel with the square obstacle in Reynolds number 50 are shown in Figure (14).

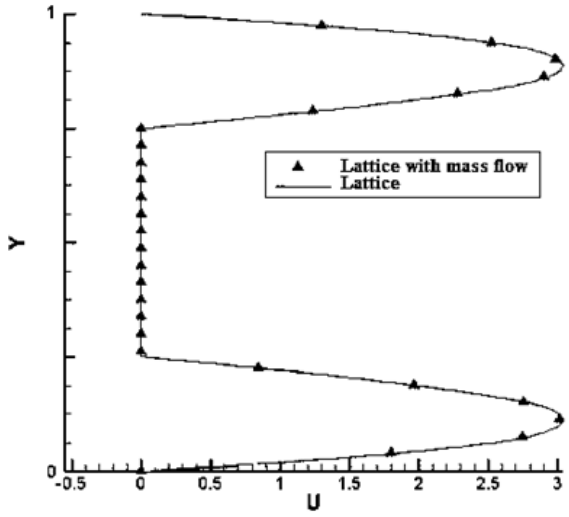

Fig. 13: Comparison of dimensionless velocity distribution (x-velocity) in a channel with an obstacle for the two states of flow rate control and without it on line (X=5, Y), for Reynolds number of 50 and mesh of 80*800

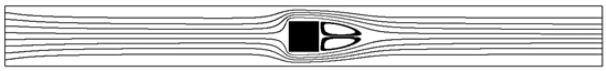

Fig. 14: Streamlines in channel with a square obstacle in Reynolds number of 50

The effect of flow rate control on fluid flow in a 90-degree bend

The flow rate control code is used not only for simple channels but also for flow inside the bent channel. Figure (15) shows a channel with a 90-degree bend and its dimensions. The total length and height of the bent channel are equal to 200 units.

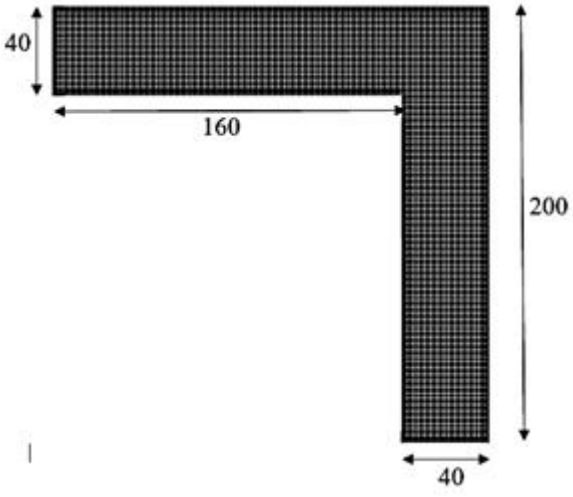

Fig. 15: Mesh and dimensions of the channel with a 90-degree bend

Figure (16) shows the boundary conditions and dimensionless parameters of the 90-degree bend channel where the X and Y are non-dimensional axes with respect to the overall length and height of the bent channel. For Reynolds's number of 30, and without the flow rate control code, the solution time is 679 seconds. By using the flow rate control code with a URF of 0.036, the solution time was reduced to 409 seconds. The stream lines of the channel in Reynolds number 30 are shown in Figure (17).

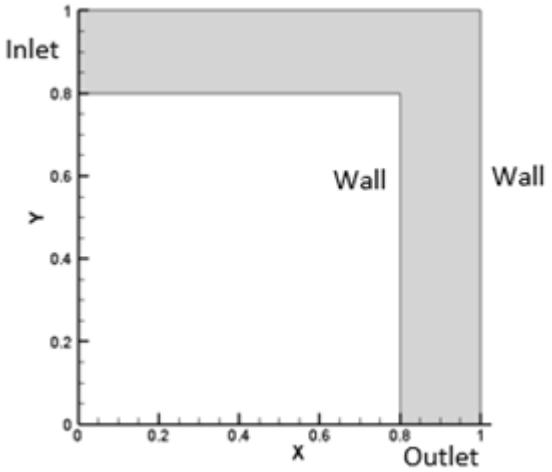

Fig. 16: Geometry of 90-degree bend with dimensionless dimensions of X and Y, and boundary conditions

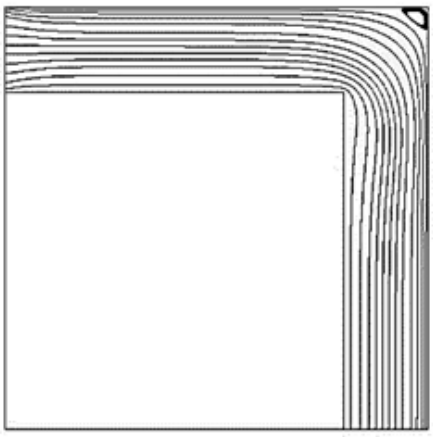

Fig. 17: Streamlines for 90-degree bend and Reynolds number of 30

Figure (18) shows the distribution of axial dimensionless velocity (x-velocity) for two states of flow rate control and without control on the line (X=0.5, Y). According to Figure (18), the results of both methods are exactly the same. Using flow rate control does not reduce the accuracy of the results but only increases the convergence rate significantly. By using this method, the solution time is reduced by more than 20%.

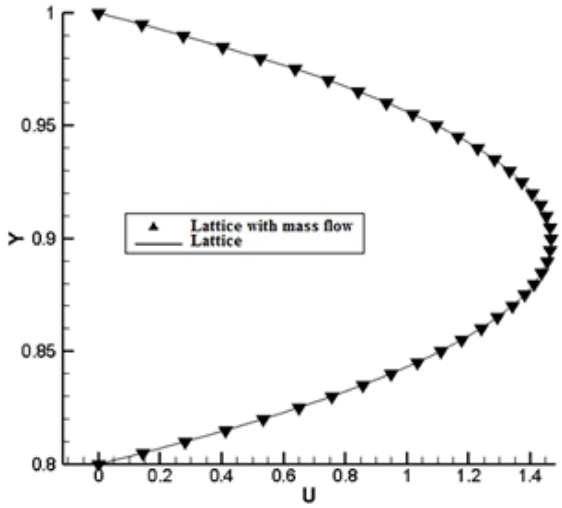

Fig. 18: Comparison of the distribution of axial dimensionless velocity for two states on the line (X=0.5, Y), Re=30 and URF=0.036.

The effect of flow rate control inside a channel with two branches

Figures (19) and (20), show the geometry and mesh of a channel with two outlets, respectively. For Reynolds number 50, the solution time of the model without control has been obtained equal to 1322 seconds, and for the state of flow rate control with URF of 0.1, the solution time of this model has been reduced to 793 seconds. In fact, this method decreases the solution time of fluid flow in a channel with two outlets to 60 percent of solution time without it. The streamlines of the channel with two branches in Reynolds number 50 are shown in Figure (21).

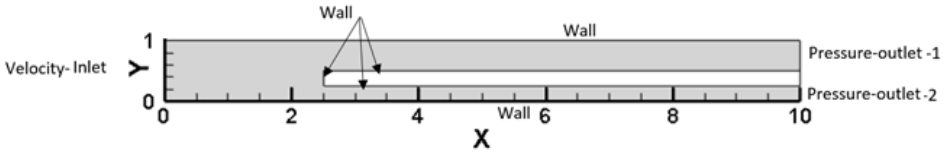

Fig. 19: Channel boundary conditions with two output boundaries with dimensionless parameters (X, Y)

Fig. 20: Mesh and dimensions of the channel with two outlets

Fig. 21: Streamlines of channel for Reynolds number of 50

Figure (22), shows the distribution of axial dimensionless velocity on the line (X=5, Y) obtained from mass flow rate control and without control. According to Figure (22), the results of these two methods are exactly congruent with each other, and the mass flow rate control method has high accuracy. The difference between the two methods is below 0.1%

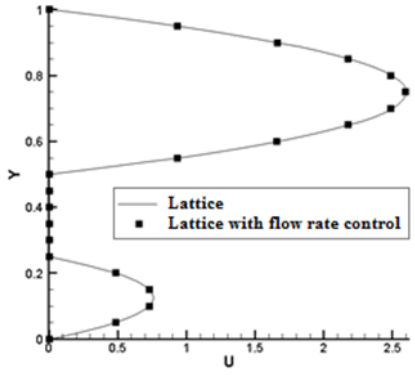

Fig. 22: Comparison of the distribution of axial dimensionless velocity for the channel with two outlets on line (X=5, Y), at Reynolds number of 50 and the flow rate control method with URF of 0.1 and without control.

Channel with obstruction

Figures (23) and (24), show geometry and mesh of a channel with obstruction at (X=5, Y), respectively. The solution time for the mass flow rate control method and Reynolds number of 50 is 3465 seconds, and without control, it is reduced to 942 seconds. The streamlines of the channel with an orifice in Reynolds number 50 have been shown in Figure (25).

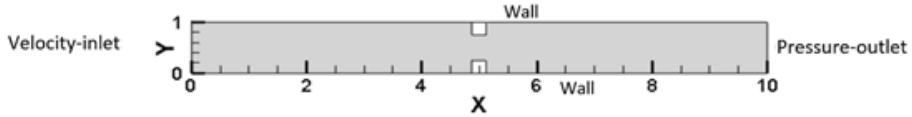

Fig. 23: Geometry and boundary conditions of a channel with obstruction with dimensionless parameters (X, Y)

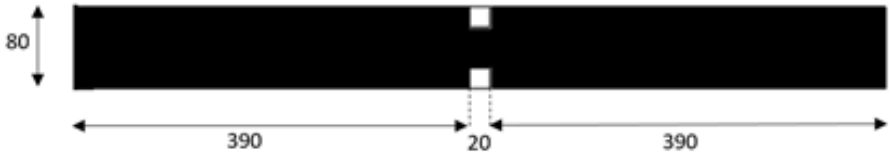

Fig. 24: Mesh and dimensions of the channel with obstruction

Fig. 25: Streamlines of channel for Reynolds number of 50

The results of these methods are compared in Figure (26). According to Figure (26), the results of these two models are congruent with each other (below 0.1%), and again, the mass flow rate control method has high accuracy in the solution of flow inside the channel with obstruction.

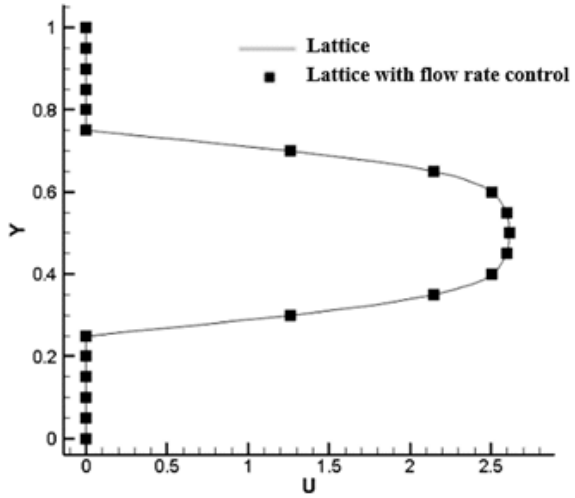

Fig. 26: Comparison of the distribution of axial dimensionless velocity for the channel with obstruction on line (X=5, Y), at Reynolds number of 50 and the flow rate control method with URF of 0.1 and without control.

Comparison with Fluent Software

Table (1), shows the comparison of solution time for different geometry between the present work, i.e., LBM with mass flow correction and solution time of Fluent software and LBM without control. Table (1) also shows the percentage difference between this work and Fluent and LBM. A negative percentage means more time to solve problems with this method compared to other methods. The solution time of the present work is less time than the fluent and conventional LBM methods. But in the 90-degree channel, due to the decrease in URF and increase in the number of meshes, the current work time is longer than the Fluent, but it has less time than the conventional LBM method.

Table 1: Comparison between solution time of present work with Fluent Software and LBM without control.

	mesh	URF	Fluent (sec.)	LBM (sec.)	this work (sec.)	% diff. with Fluent	% diff. with LBM
Channel	80×800	0.4	2064	4264	1590	29.8	168.2
Channel with obstacle	80×800	0.1	2110	4503	1623	30	177.4
bent 90	200×200	0.036	177	679	409	-56.7	66
Channel with 2 outlets	80×800	0.1	2000	1322	793	152.2	66.7
Channel with orifice	80×800	0.1	1986	3465	942	110.8	267.8

Conclusion

In this paper, a novel method based on the Lattice-Boltzmann method for decreasing the solution time of fluid flow simulation has been used. The main results are summarized below:

By using the flow rate control method, the time required for problem-solving in all of the cross sections of the domain has been decreased by two times.

- The flow rate control code not only has accurate answers in simple channels and channels with an obstacle, but it also increases convergence speed by at least two times.
- The flow rate control method, even without parallelizing the computer cores, could decrease the time required for a flow field solution.
- For channels without an obstacle, by increasing mesh elements, the time difference between flow rate control and without it has been decreased.
- The flow rate control method for all cross sections of the channel is more useful than the mass conservation method, which is considered only in the outlet of the channel.
- By increasing the Reynolds number, the solution time of the problem has been increased in usual methods; however, in the case of flow rate control methods, is declined.
- The flow rate control method has answers with high accuracy and is exactly similar to the results without flow rate control.
- To continue working and do more research in this field, it is possible to mention the development of code with the ability to perform parallel processing. Also, more complex problems, such as a cavity or step flow, can be done with the flow correction method of this work.

References

[1] A. Guittet, M. Theillard, F. Gibou, A stable projection method for the incompressible Navier-Stokes equations on arbitrary geometries and adaptive Quad/Octrees, Journal of computational physics, 292, 215–238 (2015)

[2] S.V. Patankar, D.B. Spalding, A calculation procedure for heat, mass and momentum transfer in three-dimensional parabolic flows, International Journal of Heat and Mass Transfer, 15(10), 1787–1806 (1972)

[3] H. Xiao, J. Wang, Z. Liu, W. Liu, A consistent SIMPLE algorithm with extra explicit prediction — SIMPLEC, International Journal of Heat and Mass Transfer, 120, 1255-1265 (2018)

[4] Y. Liu, F. Wang, Y. Li, Fourier analysis of the SIMPLE serials, Numerical Heat Transfer, Part B: Fundamentals, 69(3), 197-216, (2016). DOI: 10.1080/10407790.2015.1097095

[5] J. Li, Q. Zhang, Z.Q. Zhai. An efficient SIMPLER-revised algorithm for incompressible flow with unstructured grids, Numerical Heat Transfer, Part B: Fundamentals, 71(5), 425-442, (2017)

[6] M. Darwish, I. Sraj, F. Moukalled, A coupled finite volume solver for the solution of incompressible flows on unstructured grids, Journal of computational physics, 228(1), 180–201 (2009)

[7] D. Shirokoff, R.R. Rosales, An efficient method for the incompressible Navier-Stokes equations on irregular domains with no-slip boundary conditions, high order up to the boundary, Journal of computational physics, 230(23), 8619–8646 (2011)

[8] C.N. Xiao, F. Denner, B.G.M. van Wachem, Fully-coupled pressure-based finite volume framework for the simulation of fluid flows at all speeds in complex geometries, Journal of Computational Physics, 346, 91–130 (2017)

[9] M. Bayati, M. Tahmasebi Sarvestani, Numerical and Analytical Investigation of the Surface Evaporation Rate of the Different Nanofluids and Optimization Results by Using the RSM Method, Arabian Journal for Science and Engineering, (2022). DOI: 10.1007/s13369-022-07407-y.

[10] P. Nithiarasu, C.B. Liu, an artificial compressibility based characteristic based split (CBS) scheme for steady and unsteady turbulent incompressible flows. Computer Methods in Applied Mechanics and Engineering, 195(23), 2961–2982 (2006)

[11] M. Napolitano, G. Pascazio, L. Quartapelle, A review of vorticity conditions in the numerical solution of the f–w equations, Computers and Fluids, 28(2), 139–185 (1999)

[12] B. Kallemov, A. Bhalla, B. Griffith, A. Donev, An immersed boundary method for rigid bodies, Communications in Applied Mathematics and Computational Science, 11(1), 79–141 (2016)

[13] Q. Li, K.H. Luo, Q.J. Kang, Y.L. He, Q. Chen, Q. Liu, Lattice Boltzmann methods for multiphase flow and phase-change heat transfer, Progress in Energy and Combustion Science, 52, 62–105 (2016)

[14] L. An, T.S. Zhao, Transport phenomena in alkaline direct ethanol fuel cells for sustainable energy production, Journal of power sources, 341, 199–211 (2017)

[15] Q. Luo, T. Ren, D. Liang, Discretized pressure Poisson algorithm for the steady incompressible flow on a non-staggered grid, Numerical Heat Transfer, Part B: Fundamentals, 71(6), 549-559, (2017)

[16] R. Choudhury, U.J. Das, Viscoelastic effects on the three-Dimensional hydrodynamic flow past a vertical porous plate, International Journal of Heat and Technology, 31(1), 1-8 (2013). DOI: 10.18280/ijht.310101.

[17] H. Ashrafi, N. Pourmahmoud, I. Mirzaee and N. Ahmadi. Introducing a new serpentine configuration of gas channels to enhance the performance and reduce the water flooding in the PEMFC, Iranian Journal of Chemistry and Chemical Engineering, 42(1), 192-207, (2023). DOI: 10.30492/ijcce.2022.546616.5111.

[18] j. Fan, W. Duan, L. Huang, et al., High fidelity flow field reconstruction model for incompressible fluid with physical constraints, Ocean Engineering, 280, (2023). DOI: 10.1016/j.oceaneng.2023.114597.
[19] X. Chen, Z. Chai, Y. Zhao, B. Shi, Numerical Simulation of Power-Law Fluid Flow in a Trapezoidal Cavity using the Incompressible Finite-Difference Lattice Boltzmann Method, Physics Fluid Dynamics, (2023). DOI: 10.48550/arXiv.2306.07603.
[20] S. Bhopalam Rajakumar, D. Arumuga Perumal and A. Kumar Yadav, Three-dimensional simulations of fluid flows in oscillating lid-driven cavities using lattice Boltzmann method, Fluid Dynamics Research, (2023). DOI: 10.1088/1873-7005/ace37c.
[21] Y. Zhao, F. Meng and X. Lu, Improvement of lattice Boltzmann methods based on gated recurrent unit neural network. Scientific Reports Signal, Image and Video Processing (2023). https://doi.org/10.1007/s11760-023-02543-w.
[22] M. Yang, X. Li, Optimum convergence parameters of lattice Boltzmann method for predicting effective thermal conductivity, Computer Methods in Applied Mechanics and Engineering, 394, (2022). DOI: 10.1016/j.cma.2022.114891.
[23] A. Jaramillo, V. Pessoa Mapelli and L. Cabezas-Gómez, Pseudopotential Lattice Boltzmann Method for boiling heat transfer: A mesh refinement procedure, Applied Thermal Engineering, 213, (2022). DOI: 10.1016/j.applthermaleng.2022.118705.
[24] Ji-Hao Zhang, Dong-Dong Zhang, Fu-Yun Zhao & Di Liu, Non-unique steady flow solutions for pressure correction equations applied in the regime of natural convection inside free vented enclosures, Numerical Heat Transfer; Part A: Applications, 70(2), 145-161, (2016). DOI: 10.1080/10407782.2016.1173437
[25] E. Blosch, W. Shyy, R. Smith, The role of mass conservation in pressure-based algorithms. Numerical Heat Transfer, Part B Fundamentals, 24(4), 415-429 (1993)
[26] J.B. Liu, M. Bayati, M. Abbas, A. Rahimi, M. Naderi, Mesoscopic approach for simulating nanofluid flow and heat transfer in a finned multi-pipe heat exchanger, International Journal of Numerical Methods for Heat & Fluid Flow, 29(8), 2822-2839 (2019)
[27] M. Sukop, D. Or, Invasion percolation of single component, multiphase fluids with lattice Boltzmann models, Physica B: Condensed Matter, 338, 298–303 (2003)
[28] Q. Zou, X. He, On pressure and velocity boundary conditions for the lattice Boltzmann BGK model. Physics of Fluids, 9, 1591–1598 (1997)
[29] M.C. Sukop, D.T. Thorne, Lattice Boltzmann Modeling. (2006)
[30] Guide, F. U. S. Fluent Inc. Pune, India, (2005)
[31] M. Breuer, J. Bernsdorf, T. Zeiser, F. Durst, Accurate computations of the laminar flow past a square cylinder based on two different methods: Lattice-Boltzmann and finite-volume. International Journal of Heat and Fluid Flow, 21(2), 186-196 (2000)

JAST
Journal of Aerospace Science and Technology

Pages: 137- 150 / Vol. 16/ Issue 2 / Summer- Fall 2023

Journal of Aerospace Science and Technology

www:jast.ias.ir

10.22034/jast.2023.376159.1139

Submit: 10.12,2022/ Accepted: 29.07.2023

Print ISSN:2345-3648 Online ISSN: 1735-2134